CHAPTER 4

THERMAL PERFORMANCE OF TES SYSTEM WITH Al_2O_3 AND CUO NANO ADDITIVES-ORGANIC PCMS BASED NEPCMS INTEGRATED WITH IC ENGINE

This chapter has conducted comparative studies of thermophysical properties and thermal performance evaluation of the TES system integrated with the IC engine. However, the present chapter is broadly divided into three sections. The first section briefly describes the preparation method of nano-enhanced phase change materials (NEPCMs), experimental setup, procedure, and empirical correlations for conducting the experiments. The second section evaluates the thermal performance of newly designed thermal energy storage with Al_2O_3 and CuO nano additives-based capric acid, lauric acid, paraffin wax, and stearic acid nano-enhanced phase change materials (NEPCMs). Furthermore, in the last section, experimental work has been carried out for the thermal performance comparisons of Al_2O_3 and CuO nano additives in organic NEPCMs-based TES systems integrated with engine exhaust.

4.1. Preparation method for nano-enhanced phase change materials

The vol. fractions of 0.1% Al_2O_3-CuO-based capric acid, lauric acid, paraffin wax, and stearic acid NEPCM have been prepared using the one-step method. In this method, the nano-additives were mixed with melted PCM at 70°C, and the sTable and uniform dispersion of PCMs was formed with the help of a magnetic stirrer. The mixture was stirred for one hour and 30min at 70°C temperature. Lastly, the crystallization of samples

occurred at an ambient temperature, as shown in Fig. 4.1. Also, the samples of 0.1% of Al_2O_3 and CuO-based capric acid, lauric acid, paraffin wax, and stearic acid NEPCMs have been shown in Fig. 4.2.

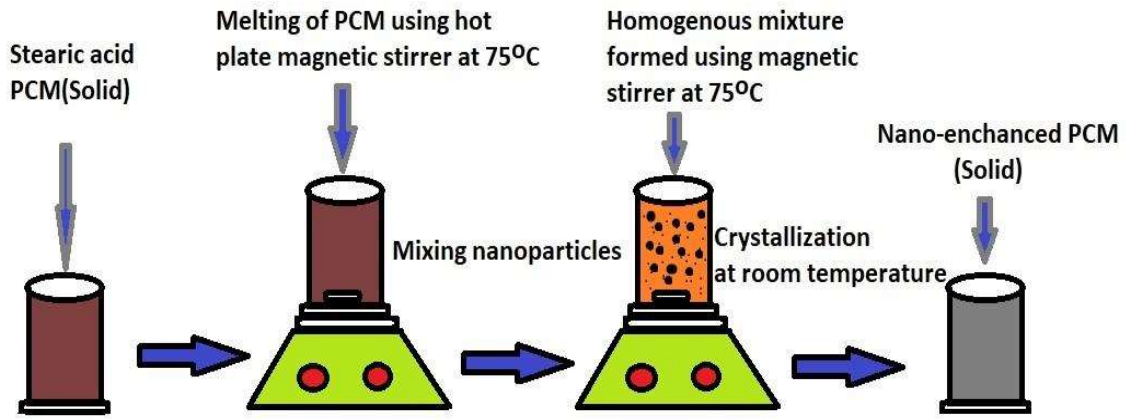

Fig.4.1. Preparation steps of nano-additives based NEPCM

Fig.4.2. Samples of Al_2O_3 and CuObased NEPCMs

After the formation of NEPCMs, the thermo-physical properties were measured by the Hot disk analyzer and presented in Table 4.1. The used TPS 508 Hot Disk Analyser

has a thermal conductivity range of 0.03 to 100W/m-K, a specific heat capacity of 5MJ/ kg-K with accuracy better than 5%.

Table 4.1: Properties obtained by the Hot disk analyzer

PCM/NEPCM	Sp. heat capacity (liquid) (kJ/kg-K)	Sp. heat capacity (solid) (kJ/kg-K)	Thermal conductivity (liquid) (W/m-K)	Thermal Conductivity (solid) (W/m-K)
CA	2.92	2.43	0.12	0.178
CA+0.1% Al_2O_3	3.21	2.78	0.183	0.196
CA+ 0.1% CuO	3.14	2.67	0.156	0.181
LA	2.35	1.98	0.126	0.174
LA+0.1% Al_2O_3	4.28	3.97	0.384	0.682
LA+ 0.1% CuO	3.64	2.52	0.220	0.389
PW	3.21	2.24	0.09	0.148
PW+0.1% Al_2O_3	5.56	4.57	0.176	4.02
PW+ 0.1% CuO	3.98	3.12	0.158	0.318
SA	2.14	1.82	0.138	0.15
SA+0.1% Al_2O_3	2.71	2.48	0.161	0.186
SA+ 0.1% CuO	3.58	3.27	0.175	0.206

4.2. Procedures of the experiment

The experimental setup is fabricated and integrated with an IC engine exhaust, a heat exchanger (shell-tubes type), and a TES system. Also, various measuring instruments such as a datalogger with the PT100 temperature sensors for temperature recording, a rotameter for a flow rate of HTF, a fluid pump, and a storage tank for HTF storage were used. In this study, stainless steel concentric tubes type TES system was coupled with the diesel engine. The diesel engine has 1396cc with a compression ratio of 21:1, four cylinders, and water-cooled was operated at 7kg and 1500rpm of engine load and speed, respectively. The TES system was filled with aluminum oxide and copper oxide nanoparticles (0.1% vol. fraction) based on capric acid, lauric acid, paraffin wax, and stearic acid PCM/NEPCMs. The diagram experiment setup is shown in Fig. 4.3. The calibrated temperature sensors were placed in a radial-axial location in the TES system, as shown in Fig. 4.4. This TES system charged with HTF, which extracted heat from the exhaust section of the engine with shell- tubes type heat exchanger.

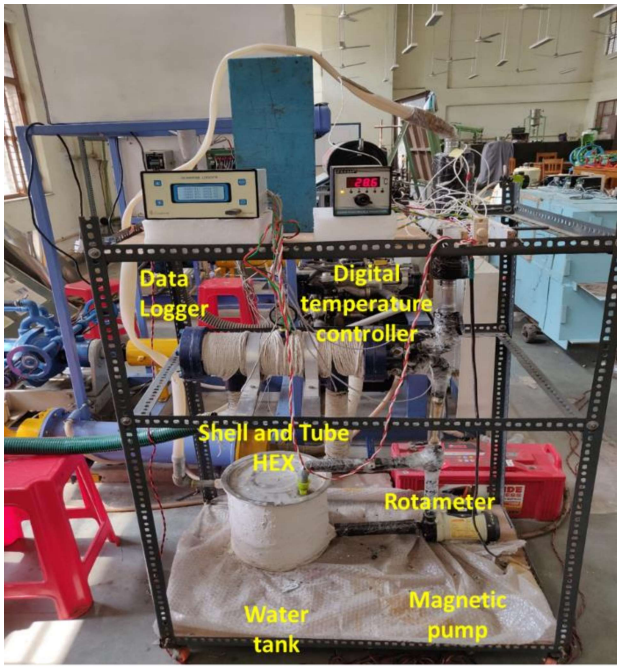

Fig.4.3. The diagram (front view) of the experiment setup

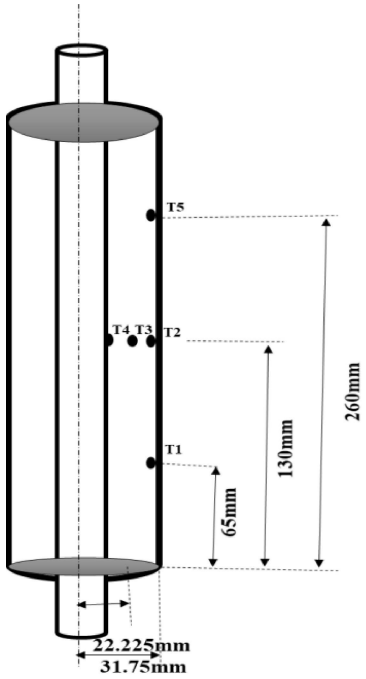

Fig.4.4. The diagram of the thermal storage system

The heat transfer fluid (HTF) was circulated with a 2LPM from the HTF tank to the TES system. The HTF tank and pipes were covered with asbestos rope and rubber tubes for leakage prevention. In a regular time interval of 10min., the temperatures at various locations have been recorded. The charging temperature of HTF and PCM/NEPCMs in the TES system has been taken as 90^{o}C.

4.3. Thermal performance evaluation of the designed experimental setup

The thermal performance of the heat exchanger and the thermal energy storage (TES) system has been evaluated. The heat exchanger was directly connected to the exhaust gases from the IC engine, and the HTF received heat from them. The experiment employed a four-stroke, 1396 CC, water-cooled diesel engine with a compression ratio of 21:1. The diesel engine's maximum power and torque are 71 Bhp at 4000 rpm and 140 Nm at 1800 rpm. The experiment has been conducted at a 7kg engine load at 1500rpm.

However, the TES system based on PCMs/NEPCMs was charged using heat from the HTF. Comparison of PCMs/NEPCMs based TES systems in axial and radial directions have been examined. Three thermocouples were placed at 65mm, 130mm, and 260mm in the axial direction from the bottom of the TES system. Furthermore, at 130mm height of the TES system, three thermocouples were placed at 12.7mm, 22.225mm, and 31.75mm in the radial direction. The charging profiles were shown the effect of nanoparticles in PCMs such as C.A., LA, PW, and S.A. In a vertical concentric tube-based TES system, natural convection of PCMs/NEPCMs was considered. The overall heat transfer coefficient of the shell and tube HEX, the heat extraction rate, the heat transfer rate, and the heat storage from HTF to PCMs/NEPCMs based TES system have all been evaluated.

4.3.1. Thermal evaluation at heat exchanger side

The following correlation has been considered for the thermal performance evaluation.

The heat transfer rate (Q_{ex}) from exhaust gases can be defined as;(Gohel, 2014)

$$Q_{ex}[kW] = \dot{m}_{ex} \times c_{pex} \times (T_{ex1} - T_{ex2}) = \dot{m}_{w} \times c_{pw} \times (T_{w2} - T_{w1}) \quad (4.1)$$

Logarithmic Mean Temperature Difference (θ_m) can be defined as (Gohel, 2014);

$$\theta_m = \frac{(\theta_1 - \theta_2)}{\ln \frac{\theta_1}{\theta_2}} \quad (4.2)$$

The overall heat transfer coefficient (U) can be defined as (Gohel, 2014);

$$U(kW/m^oC) = \frac{Q_{ex}}{A\theta_m} \tag{4.3}$$

Area of heat transfer (A) can be defined as ;

$$A[m^2] = 2 \times \pi \times r \times l \times n \tag{4.4}$$

Effectiveness (ε) of the designed thermal storage (Gohel, 2014);

$$\varepsilon = \frac{C_{ex}(T_{ex1} - T_{ex2})}{C_{min}(T_{ex1} - T_{w1})} \tag{4.5}$$

4.3.2. Thermal evaluation at thermal energy storage (TES) system side

The heat transfer rate (q) and the cumulated amount of heat storage (Q) during the charging of PCM can be expressed as (Choi et al., 1995);

$$q[kW] = m_w \times c_{pw} \times (T_{w1} - T_{w2}) \tag{4.6}$$

$$Q[kJ] = \int_0^t q \times dt \tag{4.7}$$

Percentage volume concentration (ϕ)(Senthilraja et al.,2015),

$$\phi[\%] = \left(\frac{\frac{W_{np}}{\rho_{np}}}{\frac{W_{np}}{\rho_{np}} + \frac{W_{pcm}}{\rho_{pcm}}} \right) \times 100 \tag{4.8}$$

The density of nano-PCM (Ebadi et al.,2018),

$$\rho_{np} = (1 - \phi)\rho_{pcm} + \phi\rho_p \tag{4.9}$$

Specific heat capacity of nano-PCM (Ebadi et al.,2018),

$$c_{pnp} = \frac{(1-\phi)(\rho c_p)_{pcm} + \phi(\rho c_p)_p}{\rho_{np}} \tag{4.10}$$

Thermal conductivity of nano-PCM (Ebadi et al.,2018),

$$k_{np} = \frac{k_p + 2k_{pcm} - 2\phi(k_{pcm} - k_p)}{k_p + 2k_{pcm} + \phi(k_{pcm} - k_p)} k_{pcm} \tag{4.11}$$

4.4. Comparison of nano additives in organic PCMs (CA, LA, PW & SA) based TES system integrated with IC engine

4.4.1. Effect of charging profile of nano additives-in organic PCMs based TES system

4.4.1.1. Charging profile for CA-Al_2O_3-CuO in the axial and radial direction

The charging profile in radial and axial direction for capric acid with 0.1% vol. fraction of Al_2O_3 and CuO nanoparticles based NEPCMs have been presented in Figs. 4.5(a-f). The charging time of capric acid with 0.1% vol. fraction of Al_2O_3 is 13.7% and 5.4% reduced than pure capric acid PCM and 0.1% vol. fraction of CuO nanoparticles based capric acid NEPCM. Results expressed that the heat transfer has occurred from the inner to outer of the TES system. Also, Figs. 4.5(g-h) shows the charging profiles in terms of temperature (Y-axis) variations with time (X-axis) along the axis of the pure capric acid PCM and 0.1% vol. fraction of Al_2O_3 nanoparticles based capric acid NEPCM TES system.

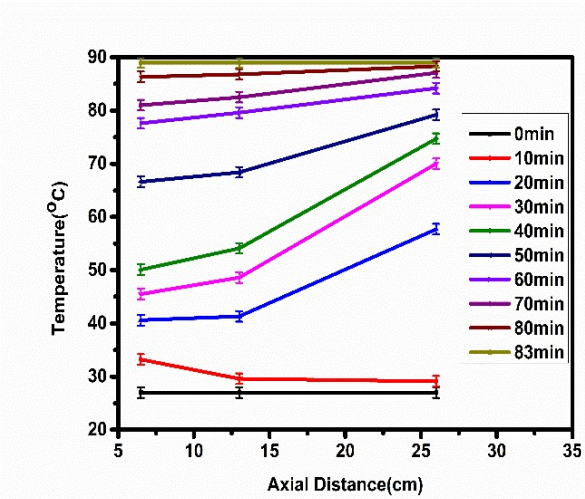

Fig.4.5(a). Charging profile of CA (axial direction)

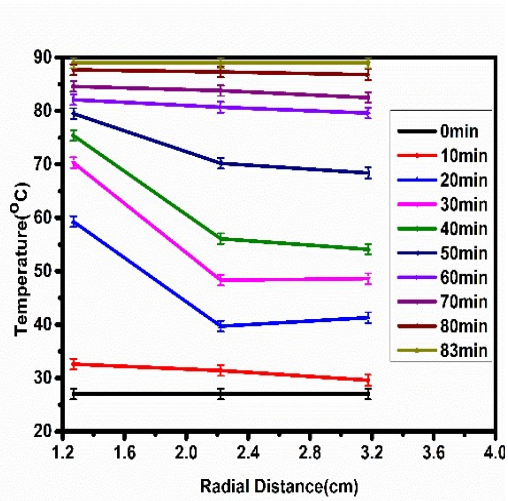

Fig.4.5(b). Charging profile of CA (radial direction)

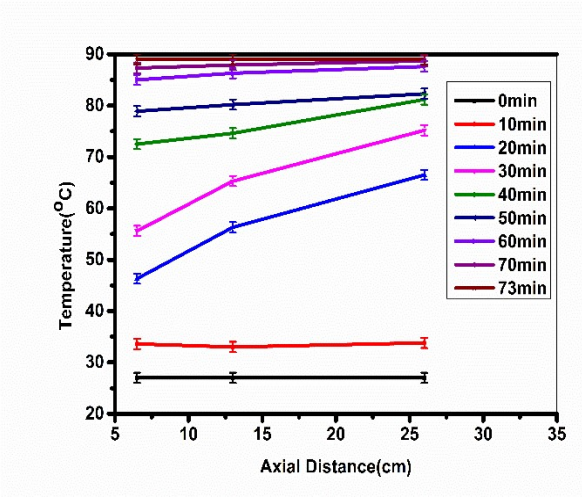

Fig.4.5(c). Charging profile of CA+Al_2O_3 (axial direction)

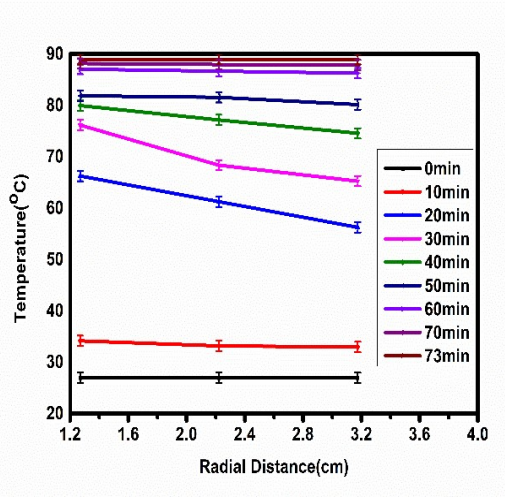

Fig.4.5(d). Charging profile of CA+Al_2O_3 (radial direction)

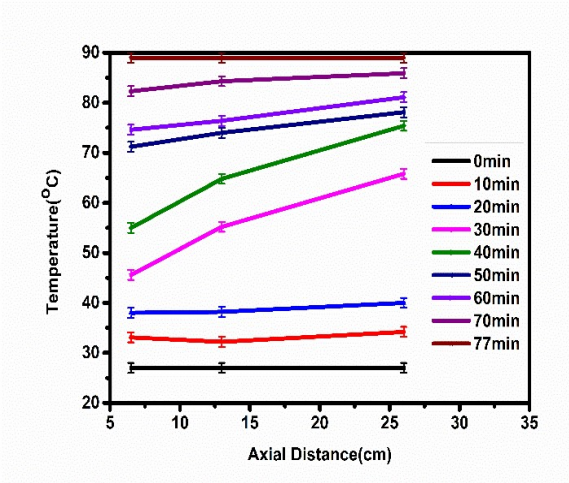

Fig.4.5(e). Charging profile of CA+CuO (axial direction)

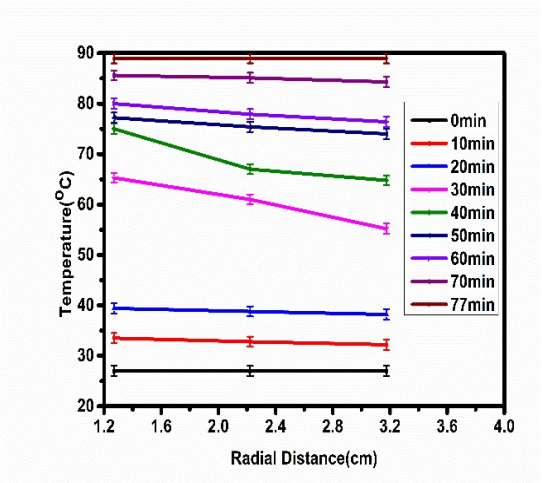

Fig.4.5(f). Charging profile of CA+CuO (radial direction)

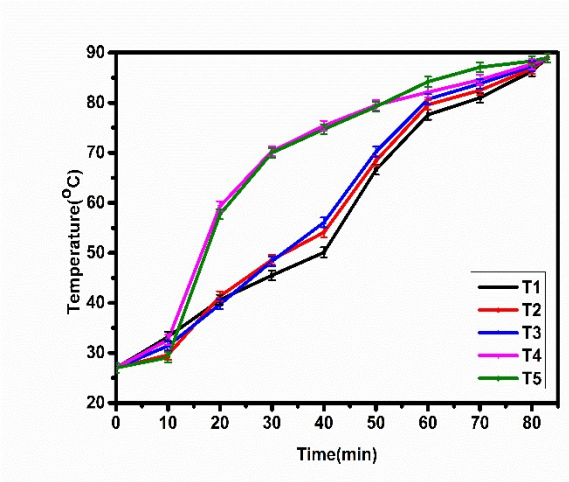

Fig.4.5(g). Charging profile of CA

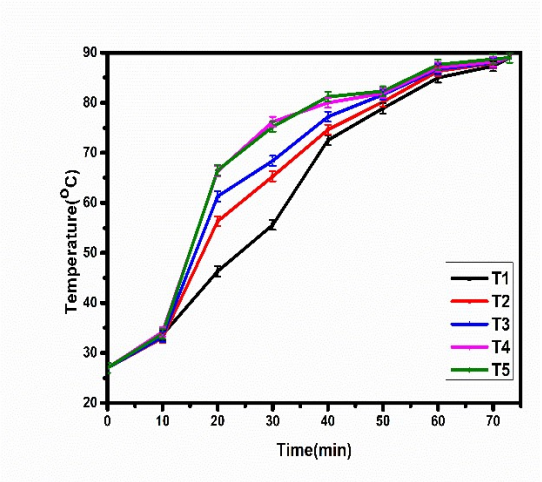

Fig.4.5(h). Charging profile of CA+Al_2O_3

Also, the maximum slope of the temperature profile has been observed in the radial direction within the time range of 20-40min., which implies that the phase change phenomena happened during this period. In the case of 0.1% vol. fraction of Al_2O_3 and CuO nanoparticles based capric acid NEPCMs, the phase change period (between 20-30min.) was reduced than pure capric acid PCM. It may happen due to a reduction in latent heat of capric acid PCM by adding Al_2O_3 and CuO nanoparticles. However, in the case of charging temperature profile in an axial direction, the slope of the curve was

maximum within a time range of 20-50min, which implied that due to the natural convection heat process, the solid phase PCM/NEPCMs were circulating top to bottom of TES system. Due to less charging time of 0.1% vol. fraction of Al_2O_3 nanoparticles based capric acid NEPCM, the slope of charging profile curve was maximum for less period (between 20-30min.) in the axial direction than 0.1% vol. fraction of CuO nanoparticles based capric acid NEPCMs and pure capric acid PCM.

4.4.1.2. Charging profile of Al_2O_3-CuO/LA in axial and radial directions

The axial and radial temperature profile of pure lauric acid PCM, Al_2O_3, and CuO nano additives-based lauric acid NEPCMs has been shown in Figs. 4.6(a-f). Results revealed that the decrease in temperature in the radial distance indicates the melting process occurred from the inner tube wall to the outer tube wall.

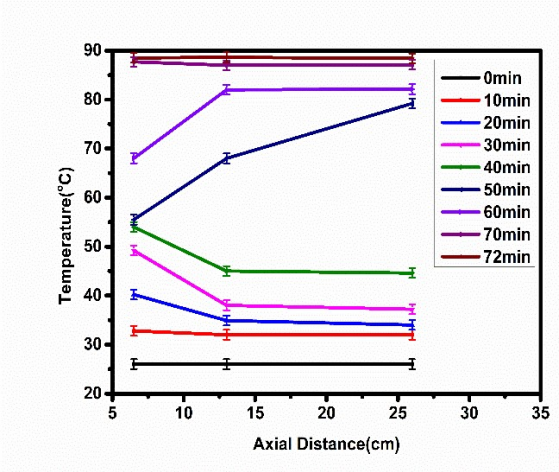

Fig.4.6(a). Charging profile of LA (axial direction)

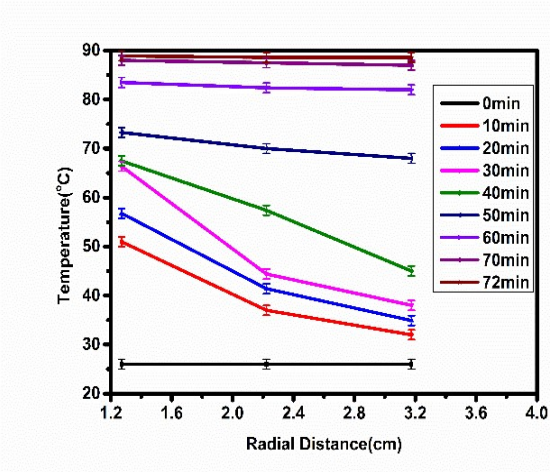

Fig.4.6(b). Charging profile of LA (radial direction)

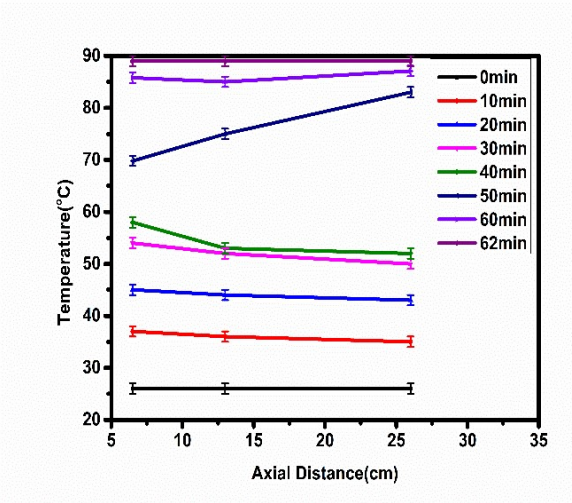

Fig.4.6(c). Charging profile of LA+Al_2O_3 (axial direction)

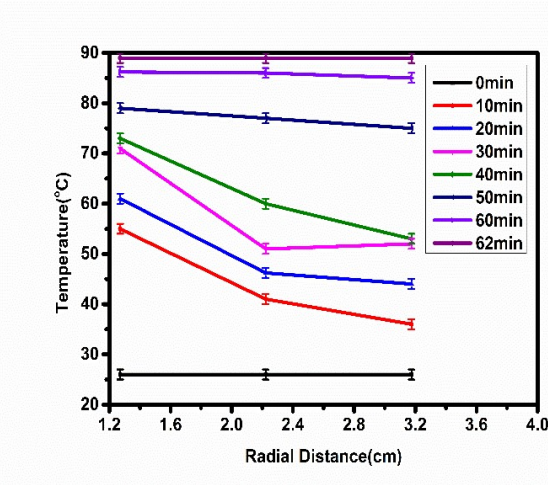

Fig.4.6(d). Charging profile of LA+Al_2O_3 (radial direction)

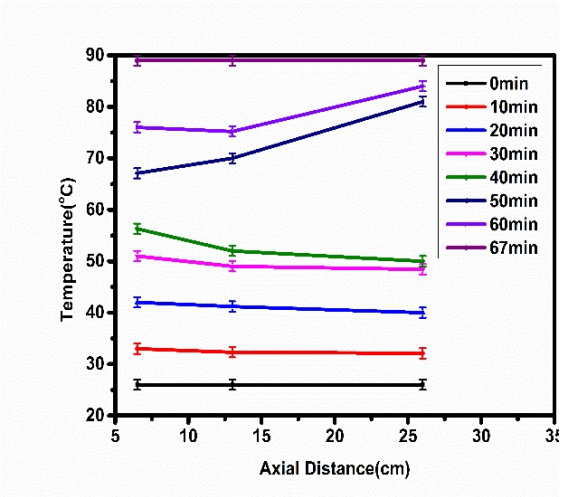

Fig.4.6(e). Charging profile of LA+CuO (axial direction)

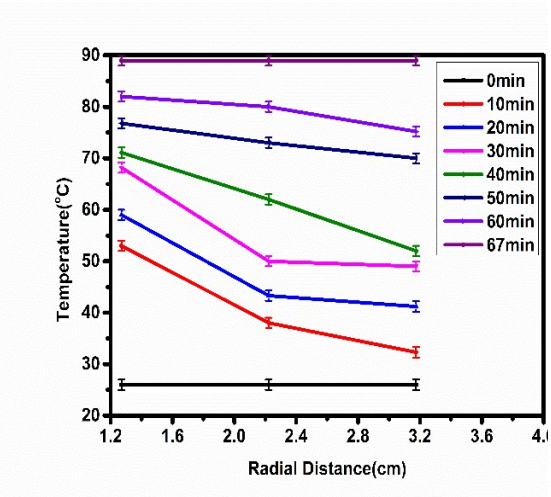

Fig.4.6(f). Charging profile of LA+CuO (radial direction)

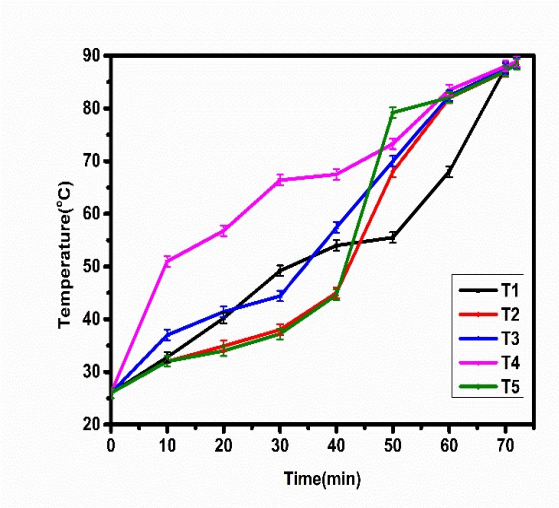

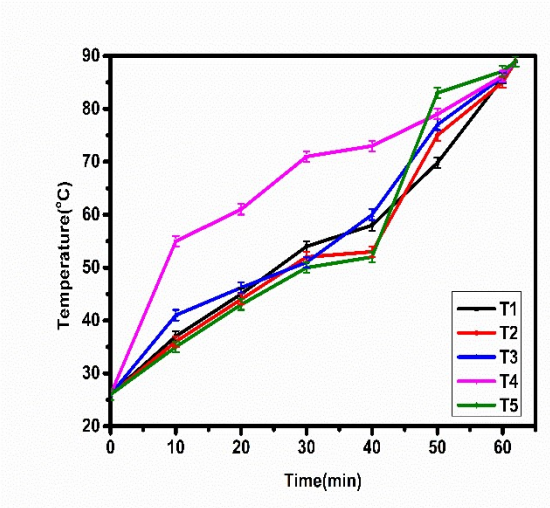

Fig.4.6(g). Charging profile of LA **Fig.4.6(h).**Charging profile of LA+Al_2O_3

However, in the radial direction, the slope of curves between the time range of 10-40min has the maximum value. Also, it has been implied that the maximum amount of PCMs/NEPCMs was in the solid phase during the time duration of 0-40min.

Furthermore, the temperature profile in the case of axial distance, within the time range of 20-40min, the temperature at the axial distance at 130mm is lower than at 65mm. The temperature at the axial distance of 130mm, after 40min, is higher than at 65mm. This may be due to the buoyancy force, the solid amount of PCM/NEPCMs settled in the bottom of the tube. The charging time of Al_2O_3 nano additives-based lauric acid PCM is lower than 10min lauric acid PCM and 5min for CuO nano additives-based lauric acid PCM, respectively. This may happen due to the more excellent thermal conductivity of Al_2O_3 nano additives based lauric acid PCM than pure lauric acid PCM and CuO nano additives based lauric acid PCM TES system. Also, Figs. 4.6(g-h) shows the charging profiles in terms of temperature (Y-axis) variations with time (X-axis) along the axis of the pure lauric acid PCM and 0.1% vol. fraction of Al_2O_3 nanoparticles based lauric acid NEPCM TES system.

4.4.1.3. Charging profile of PW, Al_2O_3-CuO-/PW in axial and radial directions

Variations in the charging temperature profile for pure paraffin wax PCM in both radial and axial directions, respectively, have been presented in Figs. 4.7(a-b). In the axial direction, the maximum deviation in temperature profile was observed within a time range of 40min.-70min. However, variations in the charging temperature profile for Al_2O_3 nano-additive based pure paraffin wax PCM in both radial and axial directions, respectively, have been presented in Figs. 4.7(c-d). In the axial direction, the maximum deviation in temperature profile was observed within a time range of 40min.-60min. And in the radial direction, significant variation is observed in the radial direction within a time range of 30min. -40min.

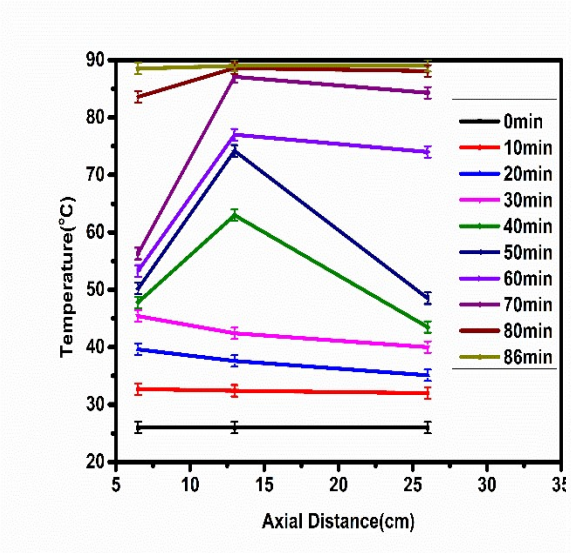

Fig.4.7(a). Charging profile of PW (axial direction)

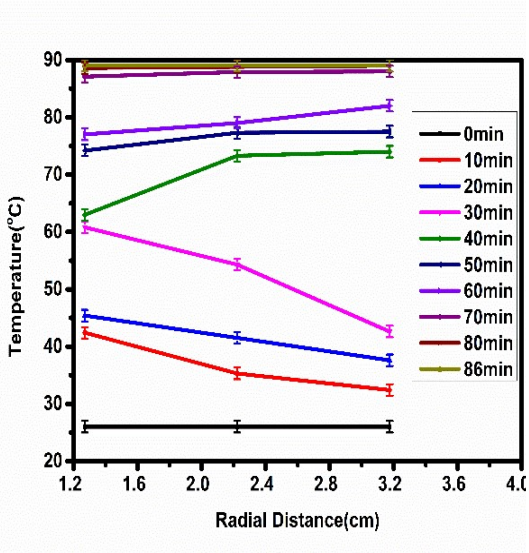

Fig.4.7(b). Charging profile of PW (radial direction)

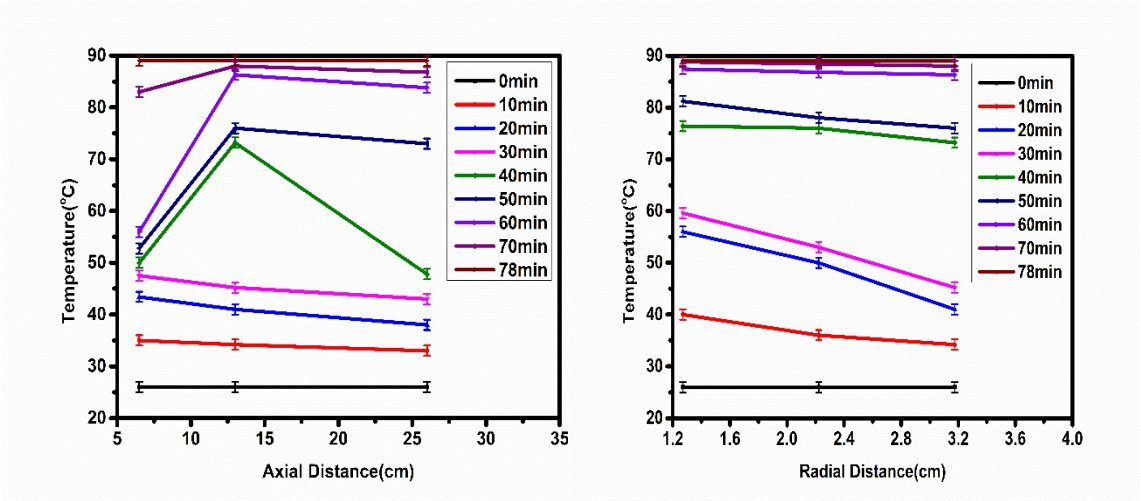

Fig.4.7(c). Charging profile of PW+Al_2O_3 (axial direction)

Fig.4.7(d). Charging profile of PW+Al_2O_3 (radial direction)

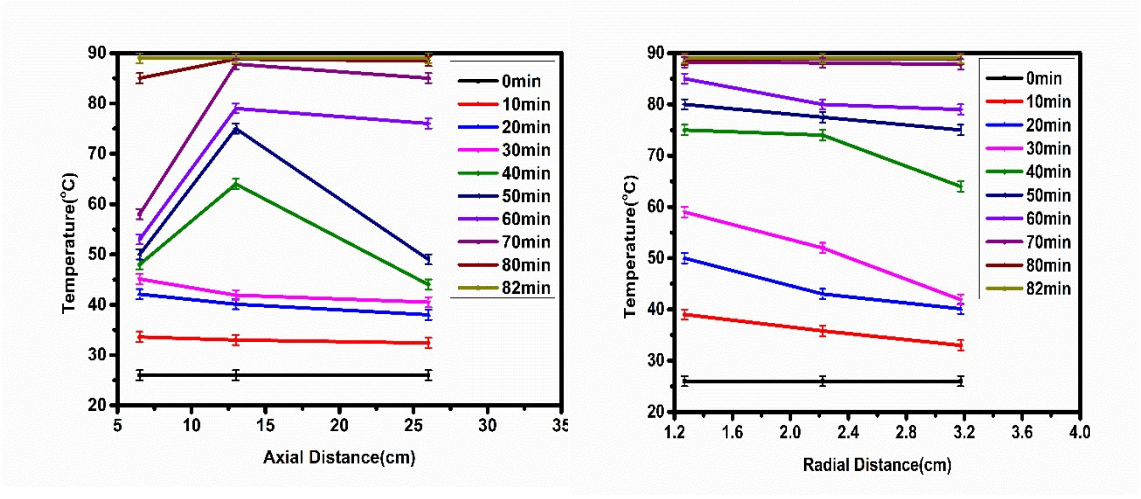

Fig.4.7(e). Charging profile of PW+CuO(axial direction)

Fig.4.7(f). Charging profile of PW+CuO (radial direction)

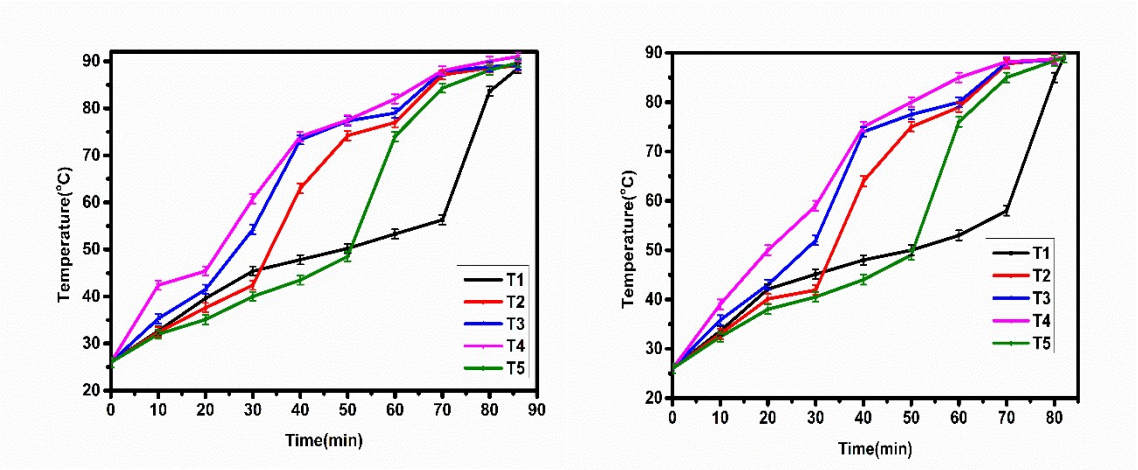

Fig.4.7(g). Charging profile of PW **Fig.4.7(h).**Charging profile of PW+Al_2O_3

The charging time of Al_2O_3 nano additives-based paraffin wax PCM is 8min lower than the paraffin wax PCM and 4min lower with CuO nano-additives-based paraffin wax PCM, as shown in Figs.4.7(e-f). However, compared to all considered samples, the 0.1% vol. fraction Al_2O_3 nano additives based lauric acid (NEPCM) required 16.13%, 8.06%, 38.71%, 25.81% and 32.26% less charging period than pure lauric acid PCM, 0.1% vol. fraction of CuO NEPCM based lauric acid, paraffin wax PCM, 0.1% vol. fraction of Al_2O_3 based paraffin wax NEPCM and 0.1% vol. fraction of CuO-based paraffin wax NEPCM, respectively. It may happen due to the lower melting time and the higher thermal conductivity of Al_2O_3 nano additives-based lauric acid PCM than other samples. Also, Figs. 4.7(g-h) shows the charging profiles in terms of temperature (Y-axis) variations with time (X-axis) along the axis of the pure paraffin wax PCM and 0.1% vol. fraction of Al_2O_3 nanoparticles based paraffin wax NEPCM TES system.

4.4.1.4. Charging profile of SA, Al_2O_3-CuO/SA in the axial and radial direction

The radial and axial charging temperature profiles of pure stearic acid, Al_2O_3, and CuO nanoparticles-based stearic acid NEPCMs are shown in Figs. 4.8(a-f). Experimental

results revealed the charging time of stearic acid with 0.1% vol. fraction of CuO is 41.53% and 13.85% reduced than pure stearic acid PCM and 0.1% vol. fraction of Al_2O_3 nanoparticles based stearic acid NEPCM, respectively. The CuO nanoparticles based on stearic acid NEPCMs required less charging time than Al2O3 and CuO nanoparticles based on capric acid NEPCMs. It may happen due to the high solidification temperature of stearic acid PCM.

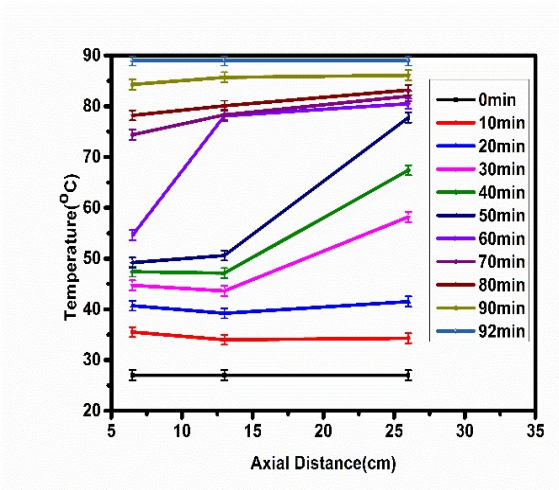

Fig.4.8(a). Charging profile of SA (axial direction)

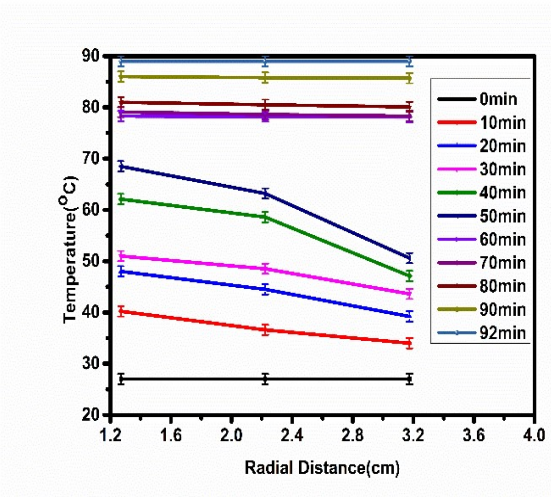

Fig.4.8(b). Charging profile of SA (radial direction)

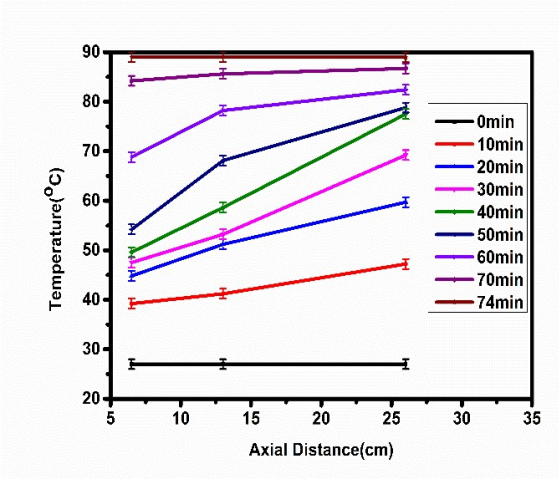

Fig.4.8(c). Charging profile of SA+Al_2O_3 (axial direction)

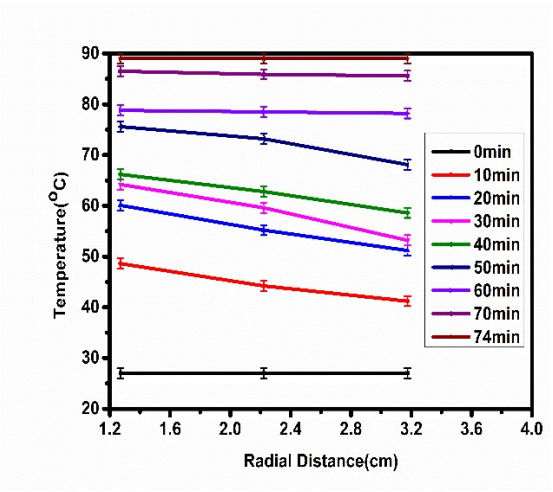

Fig.4.8(d). Charging profile of SA+Al_2O_3 (radial direction)

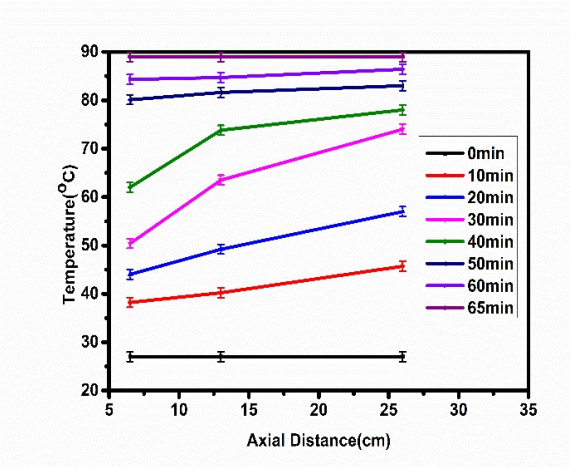

Fig.4.8(e). Charging profile of SA+CuO(axial direction)

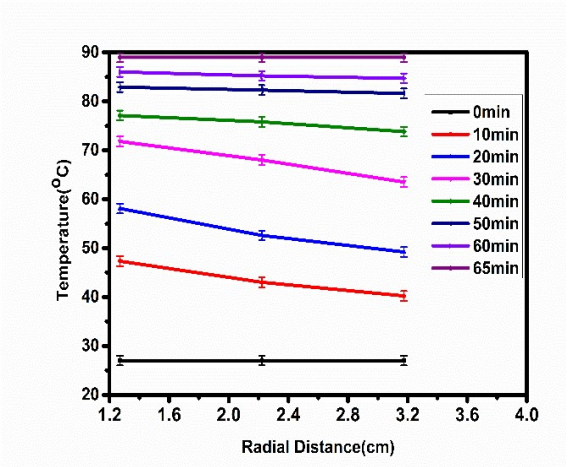

Fig.4.8(f). Charging profile of SA+CuO(radial direction)

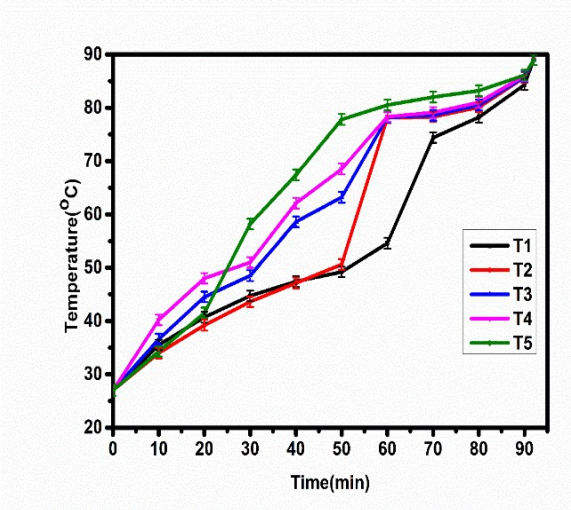

Fig.4.8(g). Charging profile of SA

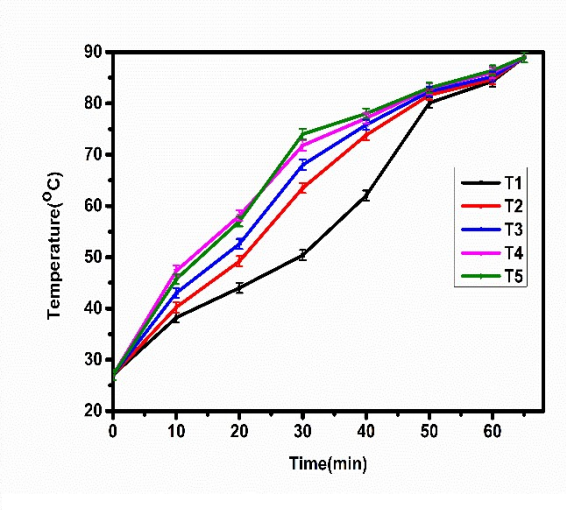

Fig.4.8(h). Charging profile of SA+CuO

Furthermore, the density of CuO nanoparticles is higher than Al_2O_3 nanoparticles. The settlement problem of CuO nanoparticles in capric acid is more than in stearic acid. But due to higher solidification temperature, CuO nanoparticles are trapped in the solid phase of stearic acid PCM. Hence, minimum CuO nanoparticles settled at the bottom of the TES system, which increased the specific capacity and thermal

conductivity of stearic acid PCM and reduced the heat of fusion. Also, Figs. 4.8(g-h) shows the charging profiles in terms of temperature (Y-axis) variations with time (X-axis) along the axis of the pure stearic acid PCM and 0.1% vol. fraction of CuO nanoparticles based stearic acid NEPCM TES system. However, the charging effectiveness of PCMs/NEPCMs-based TES systems is measured in the range of 0.51-0.625. Fluid properties govern the effectiveness of the charging in this instance.

4.4.2. Thermal performance of TES system

4.4.2.1. Effect of heat transfer coefficient of HEX

The variation in the overall heat transfer coefficient of shell-tube HEX when the TES system is filled with capric acid, lauric acid, paraffin wax, and stearic acid PCM/NEPCMs, respectively, have been presented in Figs. 4.9(a-d). The shell-tube HEX was attached to the IC engine exhaust side. The maximum overall heat transfer coefficient was observed in periods of 20min., 40 min., 40min., and 50min. The TES system is filled with CA, LA, PW, and SA PCM/NEPCMs. It may happen due to the phase change process of PCM/NEPCMs during this period, which requires a higher absorption rate of energy.

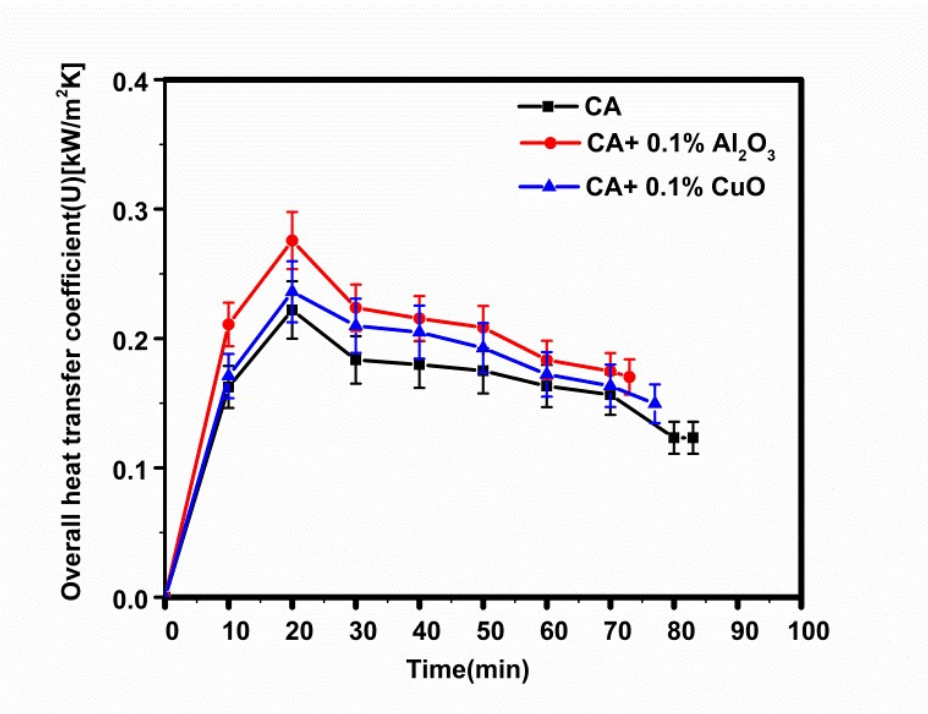

Fig.4.9(a). Overall heat transfer coefficient of capric acid with nano additives

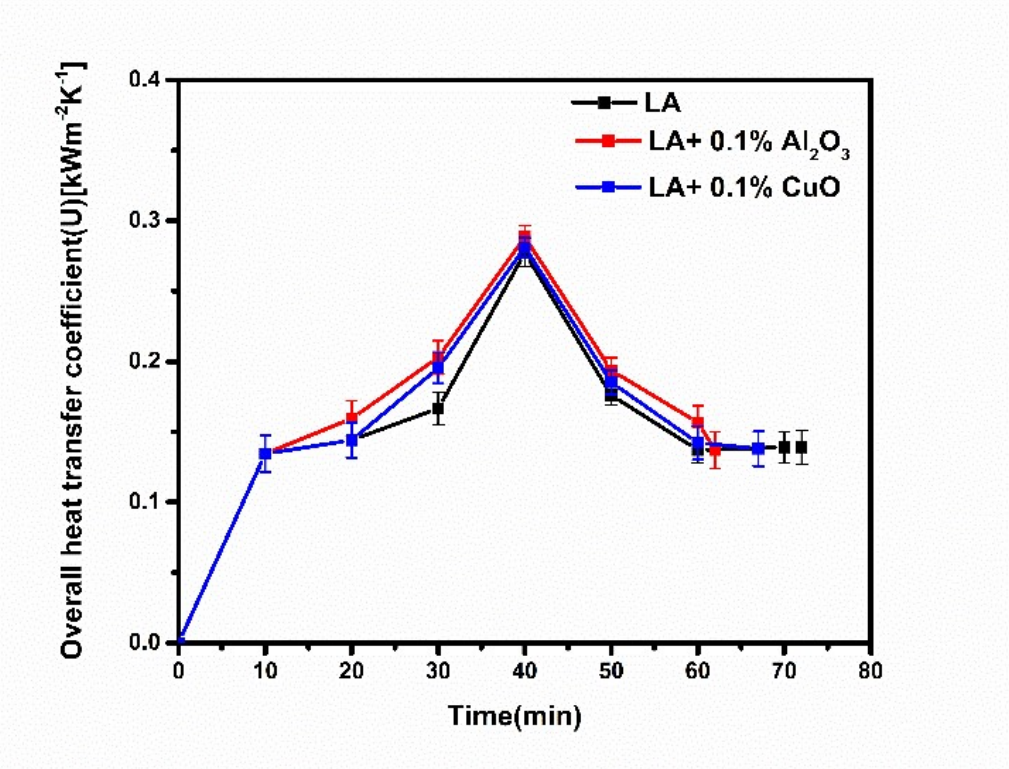

Fig. 4.9(b). Overall heat transfer coefficient of lauric acid with nano additives

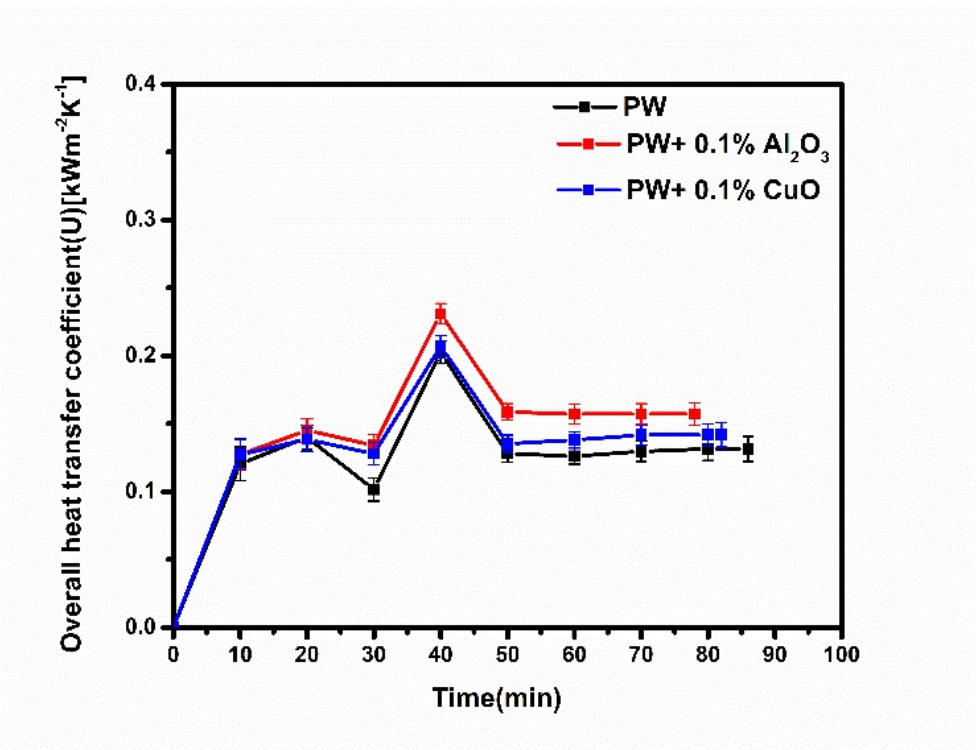

Fig. 4.9(c). Overall heat transfer coefficient of paraffin wax with nano additives

Also, results revealed that for a time period of 40min, in the Al_2O_3 nano additives based lauric acid NEPCM TES system, the overall heat transfer coefficient of shell and tube heat exchanger has 3.80%, 2.53%, 29.80%, 19.94%, and 28.33% higher values than pure lauric acid, CuO nano additives based lauric acid NEPCM, pure paraffin wax, CuO and Al_2O_3 nano additives based paraffin wax NEPCMs TES systems, respectively. However, the maximum overall heat transfer coefficient of HEX when the TES system filled with CuO nanoparticles based stearic acid NEPCM was 5.05%, 5.43%, 23.3%, 16%, and 32.2%, higher than Al_2O_3 based stearic acid and capric acid NEPCMs, CuO nanoparticles based capric acid NEPCMs, pure stearic acid, and pure capric acid PCM respectively.

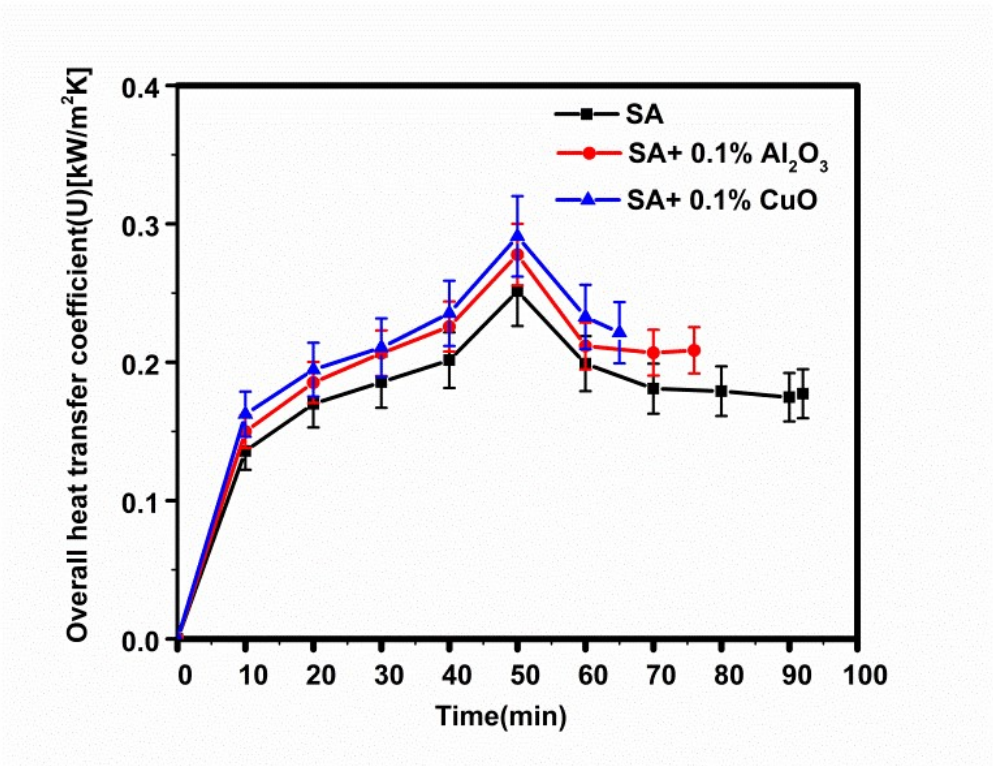

Fig. 4.9(d). Overall heat transfer coefficient of stearic acid with nano additives

4.4.2.2. Heat extraction rate (Q_e) from HTF to PCM/NEPCMs

Also, the variation in heat extraction rate though HEX integrated at the exhaust side of the IC engine when the TES system filled with capric acid, lauric acid, paraffin wax, and stearic acid PCM/NEPCMs are shown as Figs. 4.10(a-d), respectively. The result revealed that the maximum heat extraction rate of HEX when the TES system was filled with Al_2O_3 nanoparticles based capric acid NEPCM was 17.9% and 27% higher than CuO based capric acid NEPCM and pure capric acid PCM, respectively. Results revealed that at a period of 40min. Al_2O_3 nano additives based lauric acid NEPCM filled in the TES system has 7.69%, 4.61%, 38.45%, 22.57%, and 35.38% higher heat extraction rate from shell and tube heat exchanger compared to pure lauric acid, CuO-lauric acid NEPCM, pure paraffin wax, Al_2O_3, and CuO nano additives based paraffin wax NEPCMs TES system. It may be caused due to the faster rate of melting process in Al_2O_3 nano

additives-based lauric acid NEPCM in the TES system. Also, the maximum heat extraction rate of HEX when the TES system filled with CuO nanoparticles based stearic acid NEPCM was 5.21% and 22.1% higher than Al_2O_3 based stearic acid NEPCM and pure stearic acid PCM, respectively. Due to the rapid increment in temperature difference between the exhaust gas at the inlet and outlet of the shell and tube heat exchanger within 0 to 50min., the heat extraction rate increases and decreases and becomes constant. Moreover, the variation in error value for heat extraction rate was obtained to be 0.07-0.1kJ.

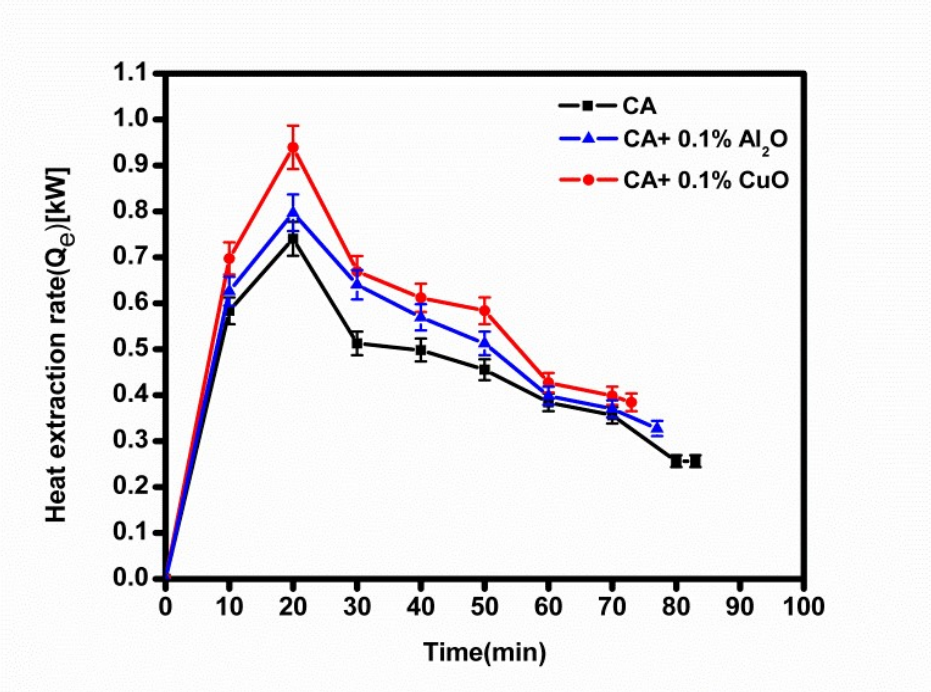

Fig.4.10(a): Heat extraction rate of capric acid with nano additives

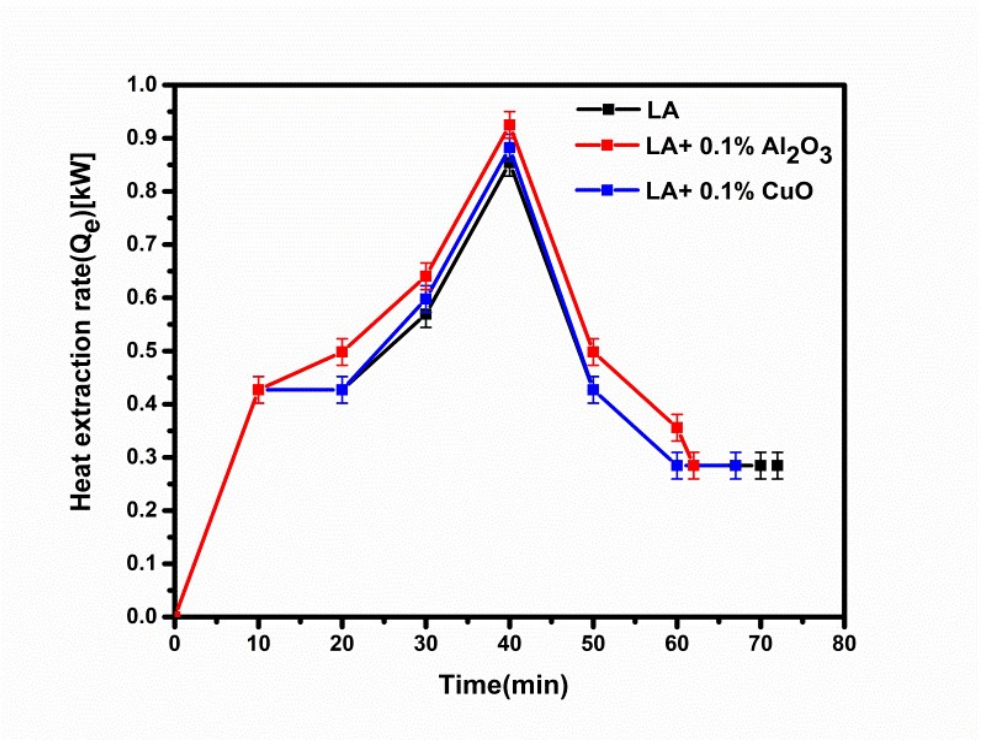

Fig.4.10(b): Heat extraction rate of lauric acid with nano additives

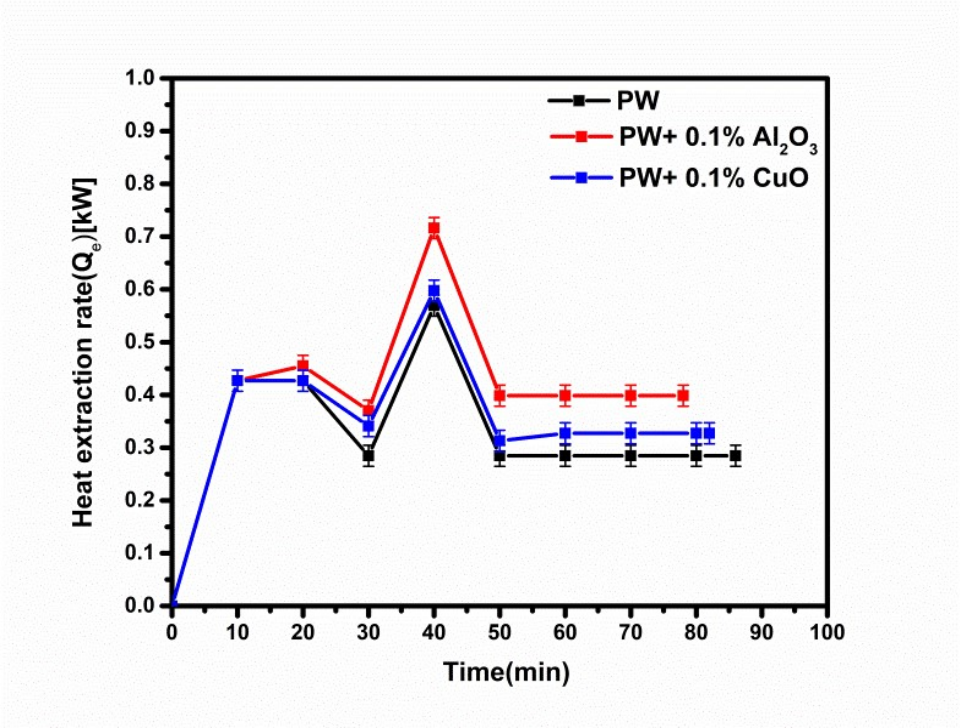

Fig. 4.10(c): Heat extraction rate of paraffin wax with nano additives

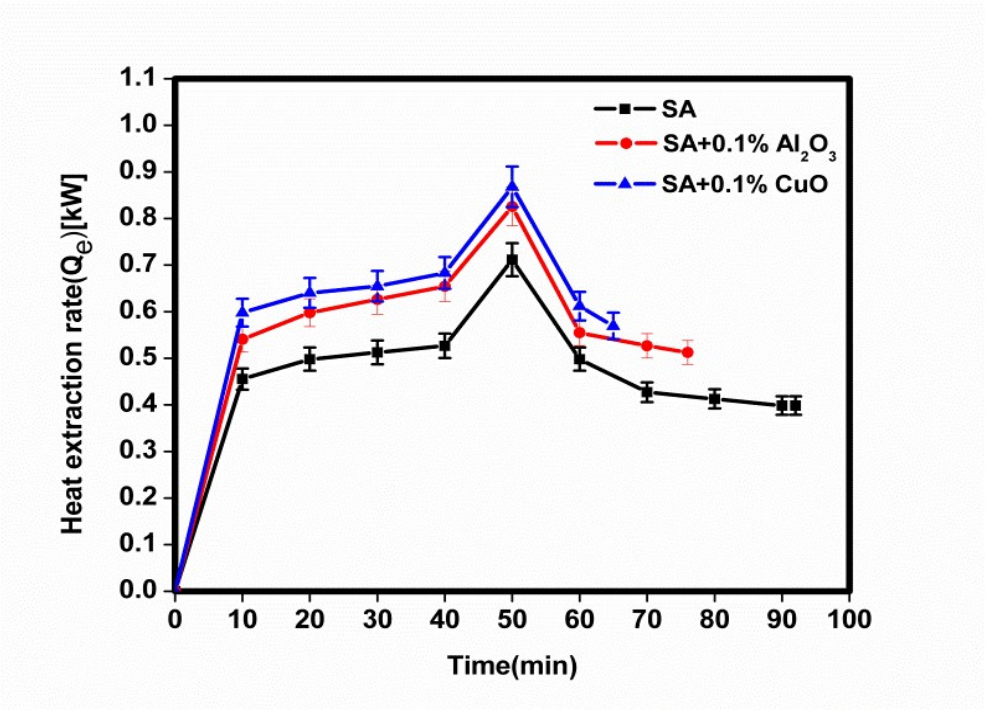

Fig. 4.10(d). Heat extraction rate of stearic acid with nano additives

4.4.2.3. Heat transfer rate of TES system

Heat transfer rate of TES systems, filled with capric acid, lauric acid, paraffin wax, and stearic acid PCM/NEPCMs, have been presented in Figs. 4.11(a-d). The experimental result revealed that Al_2O_3 nanoparticles based capric acid NEPCM has the maximum heat transfer rate of 7.14% and 11.1% higher than CuO nanoparticles based capric acid NEPCM and capric acid PCM, respectively, for a time period of 20min. Also, the heat transfer rate of pure lauric acid and nano additives-based lauric acid NEPCM increased from a period of 0min. to 20min. and then after it decreased slowly. Lauric acid with Al_2O_3 nano additives NEPCM shows a maximum heat transfer rate of 20min. than pure lauric acid and CuO nano additives-based lauric acid NEPCMs TES system. In the case of paraffin wax-based NEPCMs, a slightly different result has been observed for lauric acid PCM/NEPCM. However, the heat transfer rate of pure paraffin wax and nano

additives based on paraffin wax NEPCM increased within a period range from 0min. to 30min. and then after it decreased slowly.

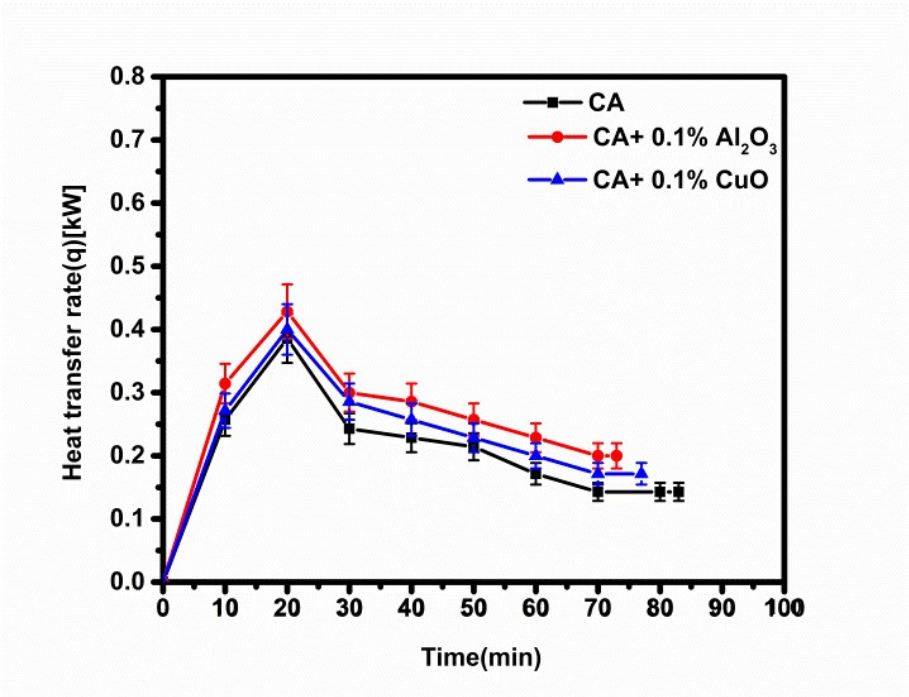

Fig. 4.11(a). Heat transfer rate of capric acid with nano additives

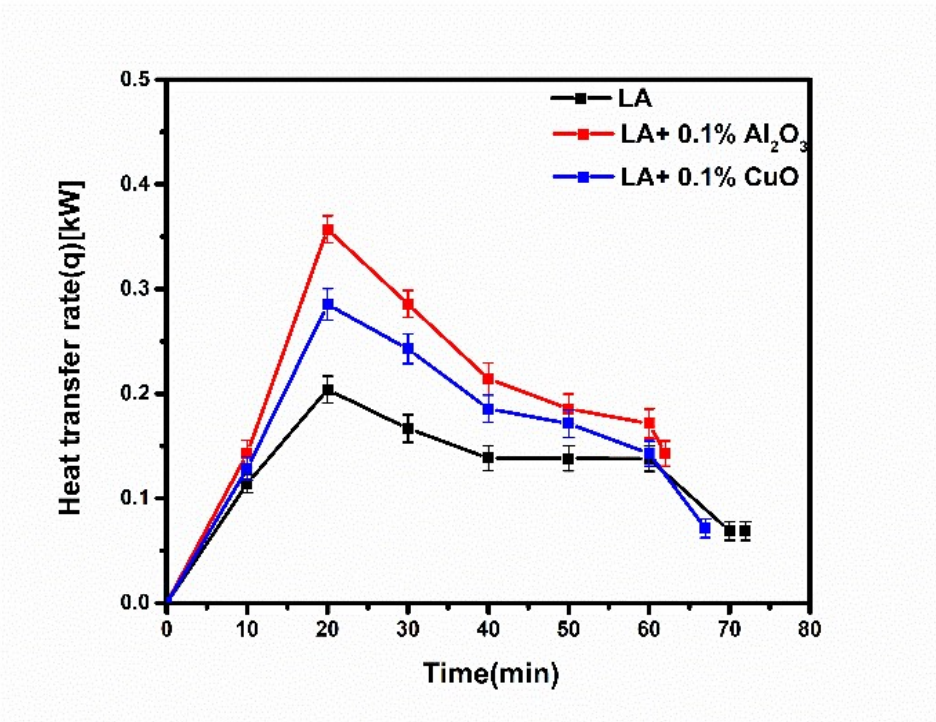

Fig. 4.11(b). Heat transfer rate of lauric acid with nano additives

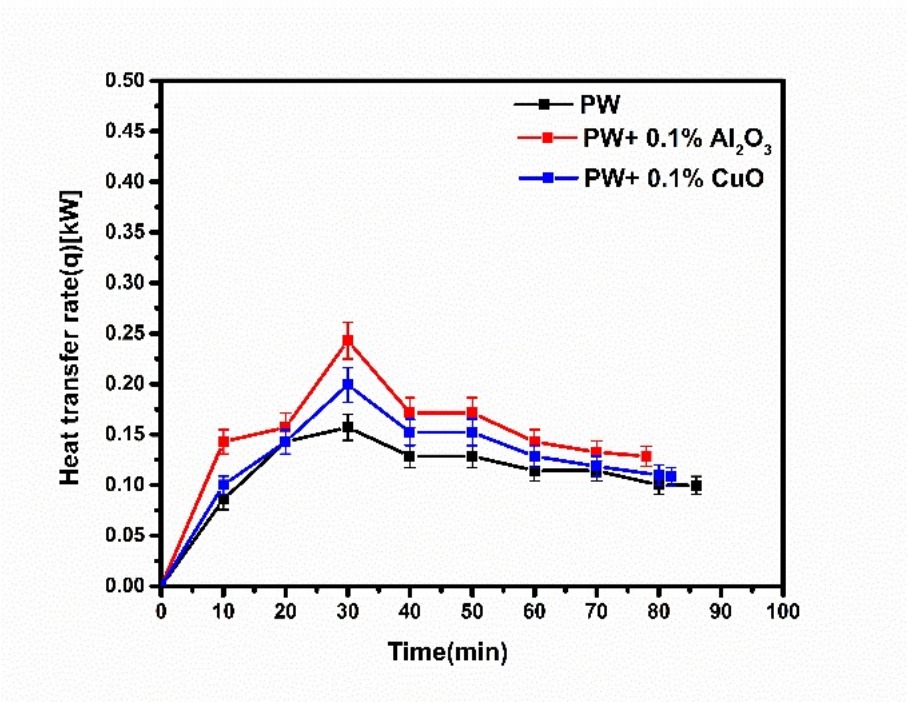

Fig. 4.11(c). Heat transfer rate of paraffin wax with nano additives

The paraffin wax with Al_2O_3 nano additives NEPCM shows a maximum heat transfer rate of 30min. than pure paraffin wax and CuO nano-additives based paraffin wax NEPCMs TES system. However, in the case of the TES system with CuO nanoparticles based stearic acid NEPCM, the maximum heat transfer rate of 7.14% and 36.4% higher than Al_2O_3 nanoparticles based stearic acid NEPCM and stearic acid PCM, respectively, for a time period of 50min.

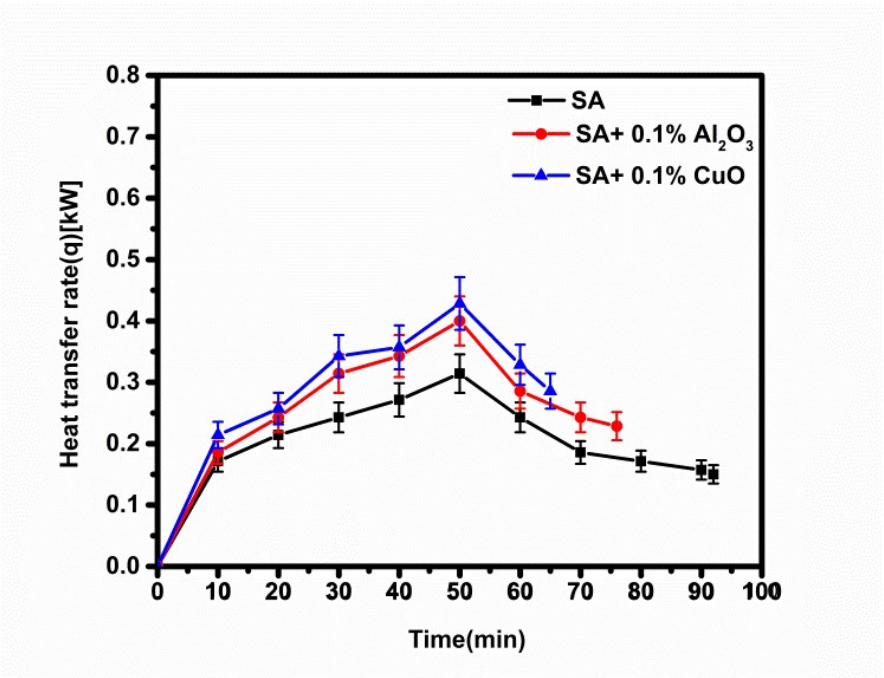

Fig. 4.11(d). Heat transfer rate of stearic acid with nano additives

4.4.2.4. Heat storage (Q) from HTF to PCM/NEPCMs

Furthermore, the cumulative heat storage of the TES system when it was filled with capric acid, lauric acid, paraffin wax, and stearic acid PCM/NEPCMs were shown in Figs. 4.12(a-d), respectively. The maximum heat storage of the TES system with Al_2O_3 nanoparticles-based capric acid NEPCM was obtained at 20min, which is 7.12%, and 11.25% higher than CuO nanoparticles-based capric acid NEPCM and capric acid PCM, respectively. In the case of lauric acid with 0.1% Al_2O_3 nanoparticles based NEPCM has greater heat storage capacity than the pure lauric acid PCM and 0.1% CuO nanoparticles based lauric acid NEPCM TES system. Furthermore, paraffin wax with 0.1% Al_2O_3 nanoparticles based NEPCM TES system has greater heat storage capacity than pure paraffin wax PCM and 0.1% CuO nanoparticles based paraffin wax NEPCM TES system integrated with engine exhaust. The maximum heat storage of the TES system with CuO nanoparticles-based stearic acid NEPCM at 50min. is 7.14% and 36.36% higher than

Al_2O_3 nanoparticles-based stearic acid NEPCM and stearic acid PCM, respectively. But it is indicated that heat transfer rate and heat storage are maximum during the phase change process compilation period. Also, it was observed that the TES system with CuO nanoparticles based on stearic acid NEPCM is stored a maximum amount than other samples. Furthermore, the variation in error value for heat storage was obtained to be 5-20kJ.

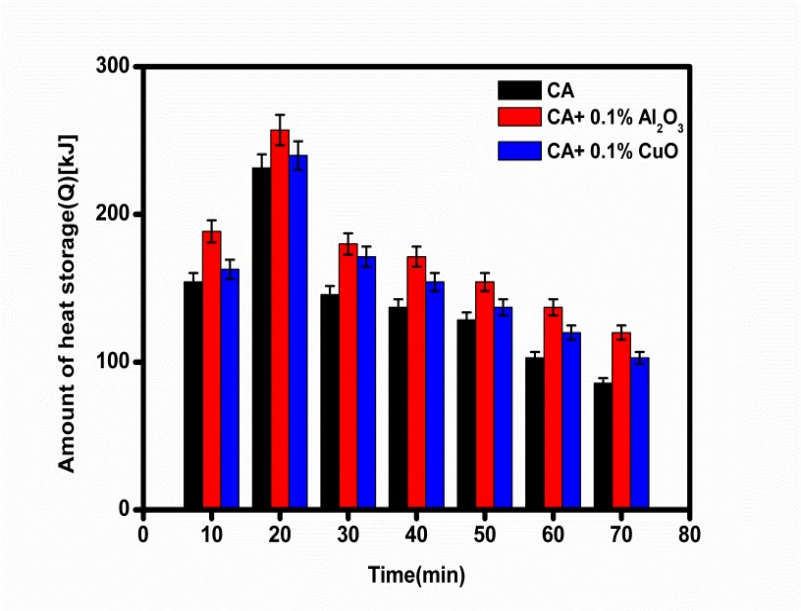

Fig. 4.12(a). Heat storage for capric acid with nano additives

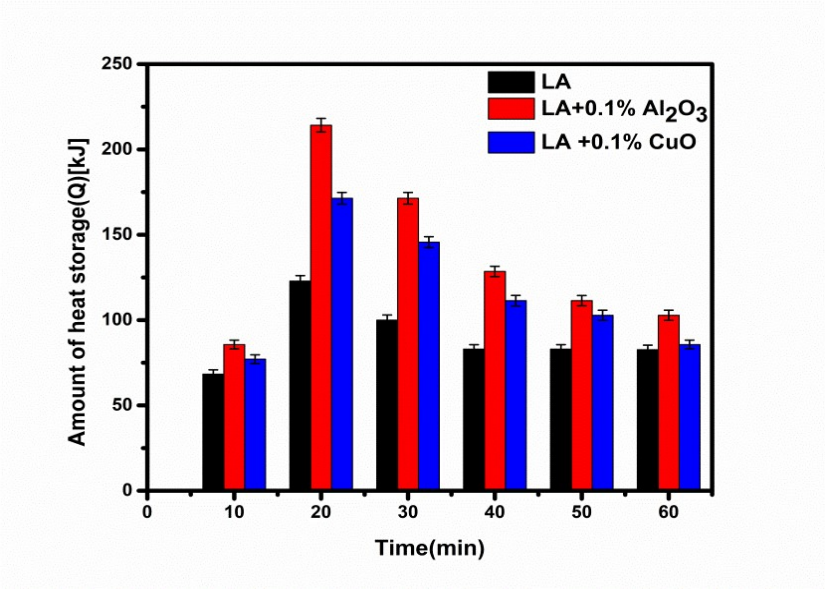

Fig. 4.12(b). Heat storage for lauric acid with nano additives

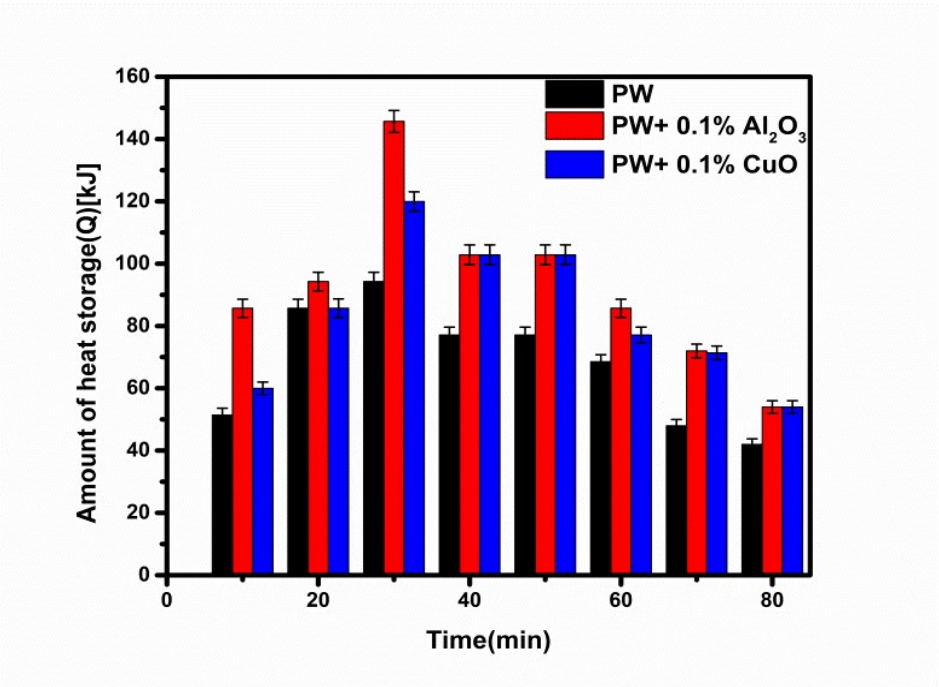

Fig. 4.12(c). Heat storage for paraffin wax with nano additives

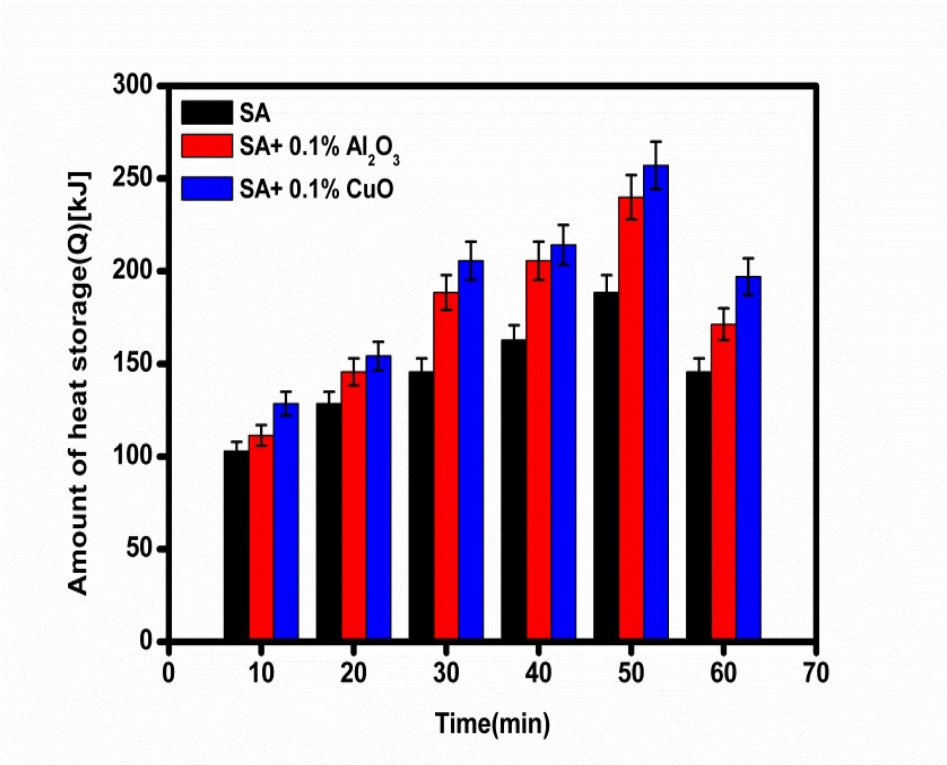

Fig. 4.12(d). Heat storage for stearic acid with nano additives

On the basis of the heat storage capacity of PCMs/NEPCMs based TES system, the energy density has also been presented in Table 4.2. Energy density is the energy storage capacity of energy storing devices per unit mass or volume.

Table 4.2: Energy density of PCMs/NEPCMs based TES system

PCMs/NEPCMs based TES system	**Energy Density(kW/kg)**	**PCMs/NEPCMs based TES system**	**Energy Density(kW/kg)**
CA	0.391	PW	0.189291
CA+Al_2O_3	0.4794	PW+Al_2O_3	0.264545
CA+CuO	0.4318	PW+CuO	0.246505
LA	0.228562	SA	0.4046
LA+Al_2O_3	0.372355	SA+Al_2O_3	0.491867
LA+CuO	0.300169	SA+CuO	0.5355

4.4.3. Energy & Exergy Analysis of NEPCM Based TES System

4.4.3.1. Energy analysis of integrated thermal storage system:

By considering the energy conservation analysis of the TES system, the charging energy efficiency of the TES system with capric acid, lauric acid, paraffin wax, and stearic acid with/without Al_2O_3 and CuO nanoparticles based NEPCM is shown in Fig. 4.13. The charging energy efficiency is the ratio of the charging rate of the thermal storage system to the heat transfer rate from the exhaust of the IC engine. The charging energy efficiency of the TES system with 0.1% Al_2O_3 nanoparticles based lauric acid NEPCM was 89.8%, 0.877%, and 87.5% higher than Al_2O_3 nanoparticles based capric acid, paraffin wax, and stearic acid, capric acid, and stearic acid NEPCM, respectively. Futhermore, The charging energy efficiency of the TES system with 0.1% Al_2O_3 nanoparticles based lauric acid

NEPCM was 91.58%, 6.07%,5.64%, and 89.9% higher than capric acid, lauric acid paraffin wax, and stearic acid, capric acid, and stearic acid PCMs, respectively. It may happen due to improvement in specific heat capacity and decrement in charging time.

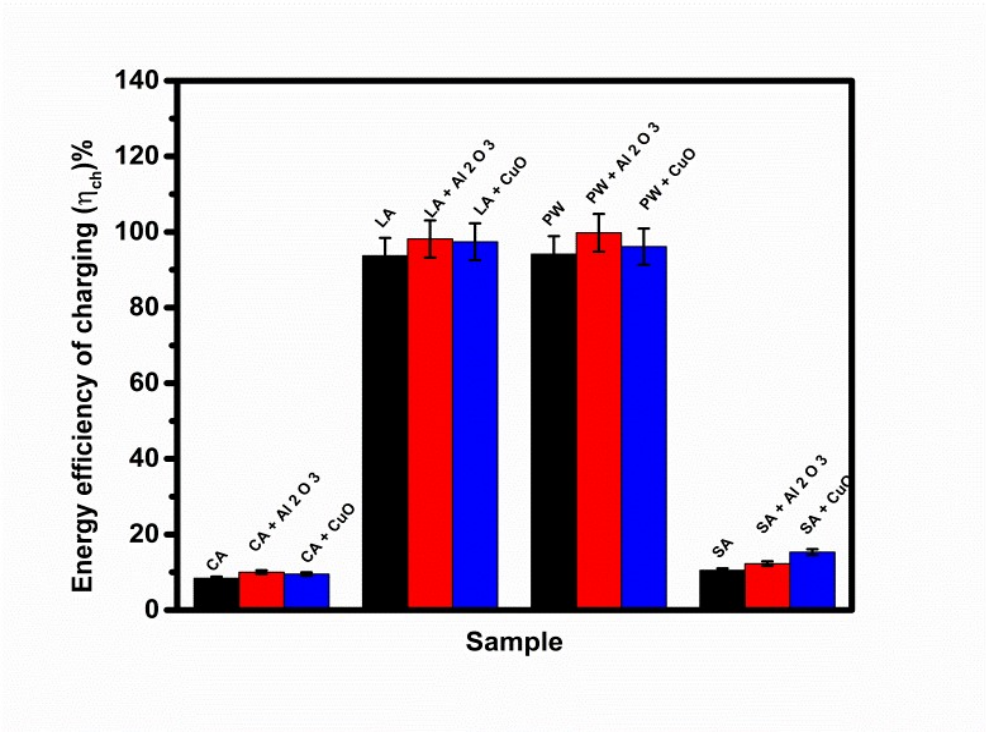

Fig.4.13. Variation of charging energy efficiency

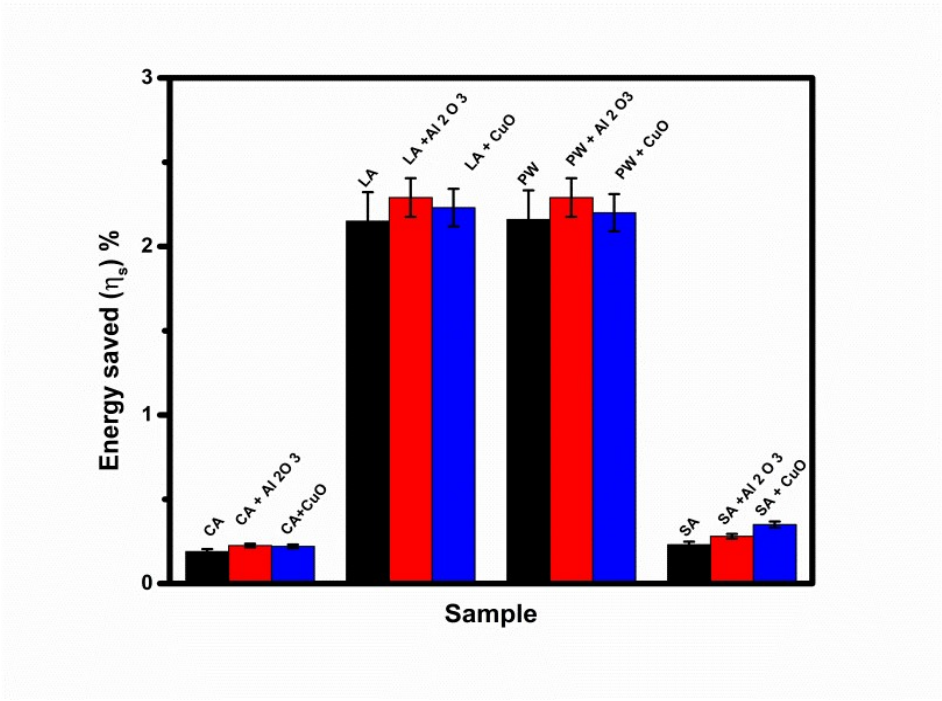

Fig.4.14. Variation of energy saved

Also, the energy saved from the exhaust, which is the ratio of the charging rate of the TES system to fuel energy, is shown in Fig. 4.14. The energy saved represents the ratio of the charging rate of the integrated TES system to the input chemical energy that is the fuel energy. The energy saved from the exhaust in case of TES filled with 0.1% Al_2O_3 nanoparticles based lauric acid NEPCM was 90.17%, 2%, and 87.77% higher than Al_2O_3 nanoparticles based capric acid, paraffin wax, and stearic acid NEPCM, respectively. Results revealed that the effect of energy analysis for an integrated TES system has an optimum value in the case of lauric acid with a 0.1% Al_2O_3 nanoparticles-based TES system. It may be caused due to the less time required for the charging and the improved value of the thermophysical properties of lauric acid PCM with 0.1% Al_2O_3 nanoparticles.

4.4.3.2. Exergy analysis of integrated thermal storage system

The exergy analysis of the TES system integrated with engine exhaust has been investigated. Fig. 4.15 and Fig. 4.16 are shown the exergy efficiency of charging and exergy saved from the exhaust. The exergy efficiency of charging is defined as the ratio of the charging rate of the TES system integrated with the IC engine to exergy lost in the exhaust gas due to the presence of the heat exchanger. The exergy efficiency of charging of TES system with Al_2O_3 nanoparticles based lauric acid was 35.04%, 4.64%, and 16.17% higher than Al_2O_3 nanoparticles based capric acid, paraffin wax, stearic acid NEPCM, respectively.

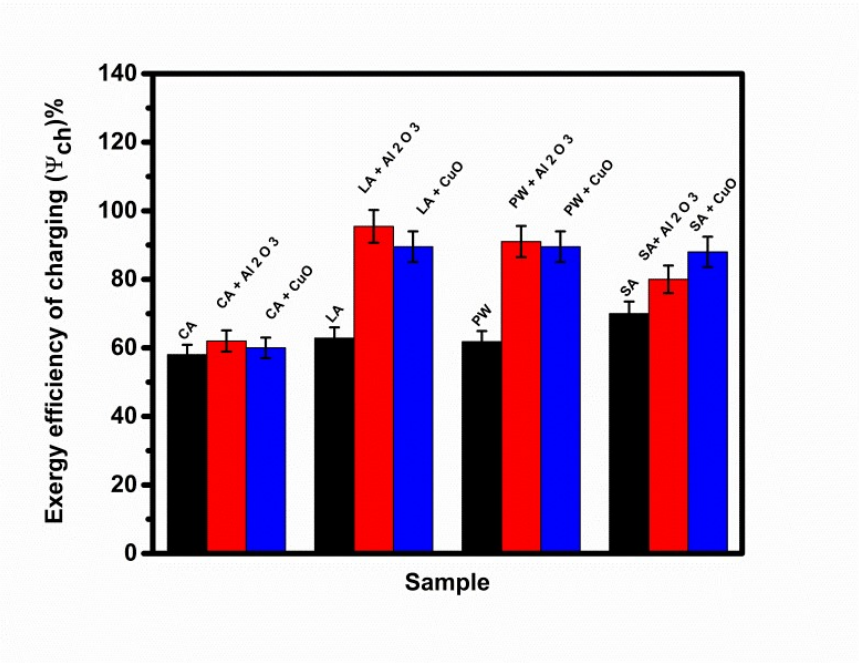

Fig.4.15. Variation of charging exergy efficiency

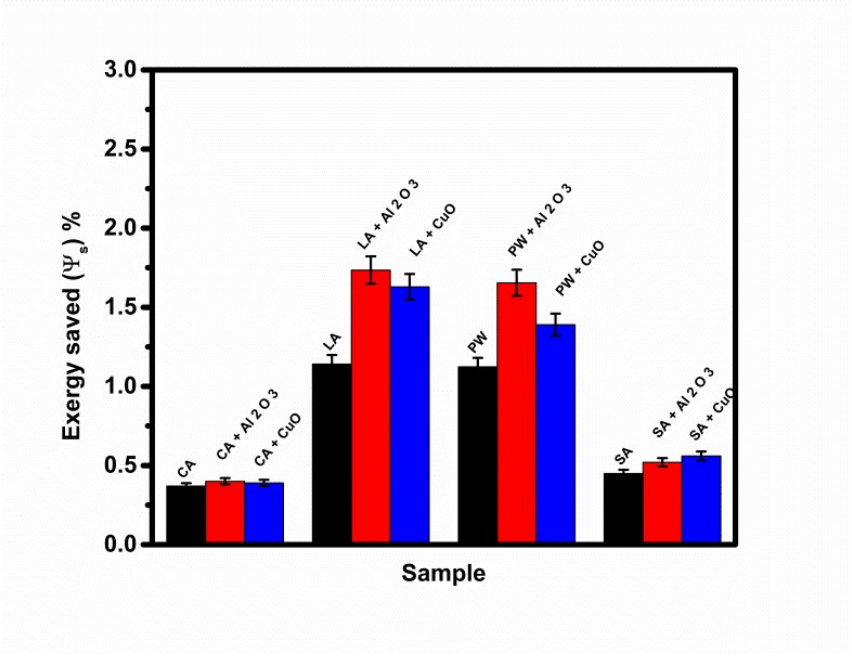

Fig.4.16. Variation of charging exergy saved

The exergy saved is denoted as the ratio of the charging rate of the TES system coupled with the CI engine to the fuel availability. The exergy saved from the exhaust in case of TES filled with Al_2O_3 nanoparticles based lauric acid was 76.94%, 4.67 %, and

70% higher than Al_2O_3 nanoparticles based capric acid, paraffin wax, stearic acid NEPCM, respectively. Furthermore, a 0.1% Al_2O_3-lauric acid NEPCM TES system integrated with the I.C engine has an optimum result for the exergy analysis.

4.5. Highlights

In this experimental study, the thermal performance of the TES system has been examined. The TES system was charged through HTF (water) at a constant flow rate of 2LPM. HTF extracted heat from exhaust gases in shell-tube HEX, integrated with I.C engine exhaust section. The experiment was conducted by filling a 0.1% volume fraction of aluminum oxide (Al_2O_3)and copper oxide (CuO) nanoparticles based on capric acid, lauric acid, paraffin wax, and stearic acid PCM/NEPCMs in a concentric tubes TES system. The following observations are obtained from the present analysis:

The energy of the storage medium of capric acid, lauric acid, and stearic acid-based TES system was increased by 122.8%, 5.66%, and 99.06%, respectively, as the mass fraction variation of PCMs from 0.1kg to 0.4 kg.

- The charging time of the TES system with vol. fraction 0.1% Al_2O_3 nanoparticles based capric acid NEPCM is 13.7% and 5.4% reduced than pure capric acid PCM and 0.1% volume fraction of copper oxide nanoparticles based capric acid NEPCM.
- The TES system is filled with 0.1% vol. fraction Al_2O_3 nano additives based lauric acid NEPCM required 16.13%, 8.06%, 38.71%, 25.81%, and 32.26% less charging period than pure lauric acid PCM, CuO-lauric acid NEPCM, paraffin wax PCM, Al_2O_3-paraffin wax NEPCM, CuO-paraffin wax NEPCM with the same vol. fraction, respectively, at 7kg engine load and 1500 engine rpm.

- In the case of capric acid, lauric acid, and paraffin wax, the maximum heat transfer and maximum amount of heat storage of the TES system were obtained with 0.1% Al_2O_3 nanoparticles based NEPCMs. But in the case of stearic acid, the TES system's maximum heat transfer and maximum amount of heat storage were obtained with 0.1% copper oxide nanoparticles-based stearic acid NEPCM, respectively.
- The energy saved with TES filled with lauric acid-based 0.1% Al_2O_3 nano-enhanced PCM TES system was 90.17%, 2%, and 87.77% higher than Al_2O_3 nanoparticles based capric acid, paraffin wax, and stearic acid NEPCM, respectively
- The exergy saved with TES filled with copper oxide nanoparticles-based stearic acid is 24.44% and 7.69%, higher than stearic acid and Al_2O_3 nanoparticles-based stearic acid NEPCM.
- The above analysis concludes that the effect of energy analysis for the integrated TES system has an optimum value in the case of lauric acid with a 0.1% Al_2O_3 nano-particles-based TES system. In the case of CuO nano-particles-based PCM, the TES system has an optimum value in the case of stearic acid with 0.1% CuO nano-particles-based TES system.